

# Study of three-body charmless $B$ decays

(The Belle collaboration)

A. Garmash<sup>2,9</sup>, K. Abe<sup>9</sup>, K. Abe<sup>41</sup>, N. Abe<sup>44</sup>, T. Abe<sup>42</sup>, I. Adachi<sup>9</sup>, H. Aihara<sup>43</sup>, Y. Asano<sup>48</sup>, T. Aso<sup>47</sup>, V. Aulchenko<sup>2</sup>, T. Aushev<sup>14</sup>, A. M. Bakich<sup>39</sup>, Y. Ban<sup>34</sup>, E. Banas<sup>28</sup>, S. Behari<sup>9</sup>, P. K. Behera<sup>49</sup>, A. Bondar<sup>2</sup>, A. Bozek<sup>28</sup>, M. Bračko<sup>21,15</sup>, T. E. Browder<sup>8</sup>, B. C. K. Casey<sup>8</sup>, P. Chang<sup>27</sup>, Y. Chao<sup>27</sup>, B. G. Cheon<sup>38</sup>, R. Chistov<sup>14</sup>, S.-K. Choi<sup>7</sup>, Y. Choi<sup>38</sup>, L. Y. Dong<sup>12</sup>, A. Drutskoy<sup>14</sup>, S. Eidelman<sup>2</sup>, V. Eiges<sup>14</sup>, F. Fang<sup>8</sup>, H. Fujii<sup>9</sup>, C. Fukunaga<sup>45</sup>, M. Fukushima<sup>11</sup>, N. Gabyshev<sup>9</sup>, T. Gershon<sup>9</sup>, A. Gordon<sup>22</sup>, K. Gotow<sup>50</sup>, R. Guo<sup>25</sup>, J. Haba<sup>9</sup>, H. Hamasaki<sup>9</sup>, F. Handa<sup>42</sup>, K. Hara<sup>32</sup>, T. Hara<sup>32</sup>, N. C. Hastings<sup>22</sup>, H. Hayashii<sup>24</sup>, M. Hazumi<sup>9</sup>, E. M. Heenan<sup>22</sup>, I. Higuchi<sup>42</sup>, T. Higuchi<sup>43</sup>, T. Hojo<sup>32</sup>, T. Hokuue<sup>23</sup>, Y. Hoshi<sup>41</sup>, K. Hoshina<sup>46</sup>, S. R. Hou<sup>27</sup>, W.-S. Hou<sup>27</sup>, H.-C. Huang<sup>27</sup>, Y. Igarashi<sup>9</sup>, T. Iijima<sup>9</sup>, H. Ikeda<sup>9</sup>, K. Inami<sup>23</sup>, A. Ishikawa<sup>23</sup>, H. Ishino<sup>44</sup>, R. Itoh<sup>9</sup>, H. Iwasaki<sup>9</sup>, Y. Iwasaki<sup>9</sup>, D. J. Jackson<sup>32</sup>, H. K. Jang<sup>37</sup>, J. H. Kang<sup>52</sup>, J. S. Kang<sup>17</sup>, P. Kapusta<sup>28</sup>, N. Katayama<sup>9</sup>, H. Kawai<sup>3</sup>, H. Kawai<sup>43</sup>, N. Kawamura<sup>1</sup>, T. Kawasaki<sup>30</sup>, H. Kichimi<sup>9</sup>, D. W. Kim<sup>38</sup>, Heejong Kim<sup>52</sup>, H. J. Kim<sup>52</sup>, H. O. Kim<sup>38</sup>, Hyunwoo Kim<sup>17</sup>, S. K. Kim<sup>37</sup>, T. H. Kim<sup>52</sup>, K. Kinoshita<sup>5</sup>, H. Konishi<sup>46</sup>, S. Korpar<sup>21,15</sup>, P. Križan<sup>20,15</sup>, P. Krokovny<sup>2</sup>, R. Kulasiri<sup>5</sup>, S. Kumar<sup>33</sup>, A. Kuzmin<sup>2</sup>, Y.-J. Kwon<sup>52</sup>, J. S. Lange<sup>6</sup>, G. Leder<sup>13</sup>, S. H. Lee<sup>37</sup>, A. Limosani<sup>22</sup>, D. Liventsev<sup>14</sup>, R.-S. Lu<sup>27</sup>, J. MacNaughton<sup>13</sup>, F. Mandl<sup>13</sup>, D. Marlow<sup>35</sup>, S. Matsumoto<sup>4</sup>, T. Matsumoto<sup>23</sup>, Y. Mikami<sup>42</sup>, H. Miyake<sup>32</sup>, H. Miyata<sup>30</sup>, G. R. Moloney<sup>22</sup>, G. F. Moorhead<sup>22</sup>, S. Mori<sup>48</sup>, T. Mori<sup>4</sup>, A. Murakami<sup>36</sup>, T. Nagamine<sup>42</sup>, Y. Nagasaka<sup>10</sup>, Y. Nagashima<sup>32</sup>, T. Nakadaira<sup>43</sup>, E. Nakano<sup>31</sup>, M. Nakao<sup>9</sup>, J. W. Nam<sup>38</sup>, Z. Natkaniec<sup>28</sup>, K. Neichi<sup>41</sup>, S. Nishida<sup>18</sup>, O. Nitoh<sup>46</sup>, T. Nozaki<sup>9</sup>, S. Ogawa<sup>40</sup>, F. Ohno<sup>44</sup>, T. Ohshima<sup>23</sup>, T. Okabe<sup>23</sup>, S. Okuno<sup>16</sup>, S. L. Olsen<sup>8</sup>, W. Ostrowicz<sup>28</sup>, H. Ozaki<sup>9</sup>, P. Pakhlov<sup>14</sup>, H. Palka<sup>28</sup>, C. S. Park<sup>37</sup>, C. W. Park<sup>17</sup>, K. S. Park<sup>38</sup>, L. S. Peak<sup>39</sup>, J.-P. Perroud<sup>19</sup>, M. Peters<sup>8</sup>, L. E. Piilonen<sup>50</sup>, K. Rybicki<sup>28</sup>, J. Ryuko<sup>32</sup>, H. Sagawa<sup>9</sup>, Y. Sakai<sup>9</sup>, H. Sakamoto<sup>18</sup>, M. Satapathy<sup>49</sup>, A. Satpathy<sup>9,5</sup>, O. Schneider<sup>19</sup>, S. Schrenk<sup>5</sup>, S. Semenov<sup>14</sup>, K. Senyo<sup>23</sup>, M. E. Seviror<sup>22</sup>, H. Shibuya<sup>40</sup>, J. B. Singh<sup>33</sup>, S. Stanič<sup>48</sup>, A. Sugiyama<sup>23</sup>, K. Sumisawa<sup>9</sup>, T. Sumiyoshi<sup>9</sup>, K. Suzuki<sup>9</sup>, S. Suzuki<sup>51</sup>, S. K. Swain<sup>8</sup>, T. Takahashi<sup>31</sup>, F. Takasaki<sup>9</sup>, M. Takita<sup>32</sup>, K. Tamai<sup>9</sup>, N. Tamura<sup>30</sup>, J. Tanaka<sup>43</sup>, M. Tanaka<sup>9</sup>, G. N. Taylor<sup>22</sup>, Y. Teramoto<sup>31</sup>, M. Tomoto<sup>9</sup>, T. Tomura<sup>43</sup>, S. N. Tovey<sup>22</sup>, K. Trabelsi<sup>8</sup>, T. Tsukamoto<sup>9</sup>, S. Uehara<sup>9</sup>, K. Ueno<sup>27</sup>, S. Uno<sup>9</sup>, Y. Ushiroda<sup>9</sup>, C. C. Wang<sup>27</sup>, C. H. Wang<sup>26</sup>, J. G. Wang<sup>50</sup>, M.-Z. Wang<sup>27</sup>, Y. Watanabe<sup>44</sup>, E. Won<sup>37</sup>, B. D. Yabsley<sup>9</sup>, Y. Yamada<sup>9</sup>, M. Yamaga<sup>42</sup>, A. Yamaguchi<sup>42</sup>, Y. Yamashita<sup>29</sup>, M. Yamauchi<sup>9</sup>, M. Yokoyama<sup>43</sup>, Y. Yuan<sup>12</sup>, C. C. Zhang<sup>12</sup>, J. Zhang<sup>48</sup>, Y. Zheng<sup>8</sup>, V. Zhilich<sup>2</sup>, and D. Žontar<sup>48</sup>

<sup>1</sup>Aomori University, Aomori

<sup>2</sup>Budker Institute of Nuclear Physics, Novosibirsk

<sup>3</sup>Chiba University, Chiba

<sup>4</sup>Chuo University, Tokyo

<sup>5</sup>University of Cincinnati, Cincinnati OH

<sup>6</sup>University of Frankfurt, Frankfurt

<sup>7</sup>Gyeongsang National University, Chinju

<sup>8</sup>University of Hawaii, Honolulu HI

<sup>9</sup>High Energy Accelerator Research Organization (KEK), Tsukuba

<sup>10</sup>Hiroshima Institute of Technology, Hiroshima

<sup>11</sup>Institute for Cosmic Ray Research, University of Tokyo, Tokyo

<sup>12</sup>Institute of High Energy Physics, Chinese Academy of Sciences, Beijing

<sup>13</sup>Institute of High Energy Physics, Vienna

<sup>14</sup>Institute for Theoretical and Experimental Physics, Moscow

<sup>15</sup>J. Stefan Institute, Ljubljana

<sup>16</sup>Kanagawa University, Yokohama

<sup>17</sup>Korea University, Seoul

<sup>18</sup>Kyoto University, Kyoto

<sup>19</sup>IPHE, University of Lausanne, Lausanne

<sup>20</sup>University of Ljubljana, Ljubljana

<sup>21</sup>University of Maribor, Maribor

<sup>22</sup>University of Melbourne, Victoria

<sup>23</sup>Nagoya University, Nagoya

<sup>24</sup>Nara Women's University, Nara

<sup>25</sup>National Kaohsiung Normal University, Kaohsiung

<sup>26</sup>National Lien-Ho Institute of Technology, Miao Li

<sup>27</sup>National Taiwan University, Taipei

<sup>28</sup>H. Niewodniczanski Institute of Nuclear Physics, Krakow

- <sup>29</sup>Nihon Dental College, Niigata  
<sup>30</sup>Niigata University, Niigata  
<sup>31</sup>Osaka City University, Osaka  
<sup>32</sup>Osaka University, Osaka  
<sup>33</sup>Panjab University, Chandigarh  
<sup>34</sup>Peking University, Beijing  
<sup>35</sup>Princeton University, Princeton NJ  
<sup>36</sup>Saga University, Saga  
<sup>37</sup>Seoul National University, Seoul  
<sup>38</sup>Sungkyunkwan University, Suwon  
<sup>39</sup>University of Sydney, Sydney NSW  
<sup>40</sup>Toho University, Funabashi  
<sup>41</sup>Tohoku Gakuin University, Tagajo  
<sup>42</sup>Tohoku University, Sendai  
<sup>43</sup>University of Tokyo, Tokyo  
<sup>44</sup>Tokyo Institute of Technology, Tokyo  
<sup>45</sup>Tokyo Metropolitan University, Tokyo  
<sup>46</sup>Tokyo University of Agriculture and Technology, Tokyo  
<sup>47</sup>Toyama National College of Maritime Technology, Toyama  
<sup>48</sup>University of Tsukuba, Tsukuba  
<sup>49</sup>Utkal University, Bhubaneswer  
<sup>50</sup>Virginia Polytechnic Institute and State University, Blacksburg VA  
<sup>51</sup>Yokkaichi University, Yokkaichi  
<sup>52</sup>Yonsei University, Seoul

We report on a study of three-body charmless decays  $B^+ \rightarrow K^+ h^+ h^-$  based on a  $29.1 \text{ fb}^{-1}$  data sample collected with the Belle detector. With no assumptions on the intermediate mechanisms, the following three-body branching fractions have been measured for the first time:  $\mathcal{B}(B^+ \rightarrow K^+ \pi^- \pi^+) = (55.6 \pm 5.8 \pm 7.7) \times 10^{-6}$  and  $\mathcal{B}(B^+ \rightarrow K^+ K^- K^+) = (35.3 \pm 3.7 \pm 4.5) \times 10^{-6}$ . We present the first observation of the decay  $B^+ \rightarrow f_0(980)K^+$  with a branching fraction product of  $\mathcal{B}(B^+ \rightarrow f_0(980)K^+) \times \mathcal{B}(f_0(980) \rightarrow \pi^+ \pi^-) = (9.6_{-2.3-1.5-0.8}^{+2.5+1.5+3.4}) \times 10^{-6}$ . This is the first reported example of a  $B$  meson decay to a scalar pseudoscalar final state. We also report the first observation of  $B^+ \rightarrow K^*(892)^0 \pi^+$  decay with a branching fraction of  $\mathcal{B}(B^+ \rightarrow K^*(892)^0 \pi^+) = (19.4_{-3.9-2.1-6.8}^{+4.2+2.1+3.5}) \times 10^{-6}$ .

PACS numbers: 13.20.He, 13.25.Hw, 13.30.Eg, 14.40.Nd

## I. INTRODUCTION

During the last few years, a considerable amount of new information on charmless hadronic decays of  $B$  mesons has been reported, primarily by the CLEO Collaboration. The discoveries of the  $B \rightarrow K\pi$  and  $B \rightarrow \pi\pi$  decay modes [1] have provided a real basis for searches for direct CP-violating effects in the  $B$  meson system.

However, because of large combinatoric backgrounds, studies of charmless  $B$  decays have concentrated mainly on two-body decay processes. Three-body decays could significantly broaden the study of  $B$  meson decay mechanisms and provide additional possibilities for direct CP violation searches. In this paper, we report the results of a study of charged  $B$  meson decays to three charged particle final states  $K\pi\pi$ ,  $KK\pi$ , and  $KKK$ , where no assumptions are made about intermediate hadronic resonances. We also present the results of a study of quasi-two-body intermediate states in the  $K^+\pi^+\pi^-$  and  $K^+K^+K^-$  final states. The inclusion of charge conjugate states is implicit throughout this work.

The data sample used for this analysis was collected with the Belle detector operating at the KEKB asymmetric energy  $e^+e^-$  collider [2]. It consists of  $29.1 \text{ fb}^{-1}$  taken at the  $\Upsilon(4S)$  resonance, corresponding to  $31.3 \times 10^6$  produced  $B\bar{B}$  pairs, and  $2.3 \text{ fb}^{-1}$  taken 40 MeV below the  $B\bar{B}$  production threshold to perform systematic studies of the  $e^+e^- \rightarrow q\bar{q}$  background.

## II. THE BELLE DETECTOR

The Belle detector [3] is a large-solid-angle spectrometer based on a 1.5 T superconducting solenoid magnet. Charged particle tracking is provided by a three layer double-sided silicon vertex detector (SVD) and a 50 layer cylindrical drift chamber (CDC) that surround the interaction region. The charged particle acceptance covers the laboratory polar

angle between  $\theta = 17^\circ$  and  $150^\circ$ , corresponding to about 92% of the full solid angle in the center-of-mass (c.m.) frame. The momentum resolution is determined from cosmic rays and  $e^+e^- \rightarrow \mu^+\mu^-$  events to be  $\sigma_{p_t}/p_t = (0.30 \oplus 0.19p_t)\%$ , where  $p_t$  is the transverse momentum in GeV/ $c$ .

Charged hadron identification is provided by  $dE/dx$  measurements in the CDC, an array of 1188 aerogel Čerenkov counters (ACC), and a barrel-like array of 128 time-of-flight scintillation counters (TOF). At large momenta ( $> 2.5$  GeV/ $c$ ) only the ACC and  $dE/dx$  are used for separation of charged pions and kaons since here the TOF provides no additional discrimination.

Electromagnetic showering particles are detected in an array of 8736 CsI(Tl) crystals that is located in the magnetic volume and covers the same solid angle as the charged particle tracking system. The energy resolution for electromagnetic showers is  $\sigma_E/E = (1.3 \oplus 0.07/E \oplus 0.8/E^{1/4})\%$ , where  $E$  is in GeV. Electron identification in Belle is based on a combination of  $dE/dx$  measurements in the CDC, the response of the ACC, and the position, shape and total energy deposition (i.e.  $E/p$ ) of the shower registered in the calorimeter. The electron identification efficiency is greater than 92% for tracks with  $p_{\text{lab}} > 1.0$  GeV/ $c$  and the hadron misidentification probability is below 0.3%.

The magnetic field is returned via an iron yoke that is instrumented to detect muons and  $K_L$  mesons. We use a Monte Carlo simulation to model the response of the detector and determine acceptance [4].

### III. EVENT SELECTION

Charged tracks are required to satisfy a set of track quality requirements based on the average hit residual and on the distances of closest approach to the interaction point in the plane perpendicular to the beam and the plane containing the beam and the track. We also require that the transverse track momenta be greater than 0.1 GeV/ $c$  to reduce the low momentum combinatoric background.

Charged kaon candidate tracks are selected with a set of PID criteria that has about 90% efficiency, a charged pion misidentification probability of about 8%, and a negligible contamination from protons. We also reject tracks that are identified as electrons. Since the muon identification efficiency and fake rate vary significantly with the track momentum, we do not reject muons to avoid additional systematic error.

We reconstruct  $B$  mesons in three charged track final states with at least one positively identified kaon. The candidate events are identified by their c.m. energy difference,  $\Delta E = (\sum_i E_i) - E_b$ , and the beam constrained mass,  $M_{bc} = \sqrt{E_b^2 - (\sum_i \vec{p}_i)^2}$ , where  $E_b = \sqrt{s}/2$  is the beam energy in the c.m. frame, and  $\vec{p}_i$  and  $E_i$  are the c.m. three-momenta and energies of the candidate  $B$  meson decay products. We select events with  $M_{bc} > 5.20$  GeV/ $c^2$  and  $|\Delta E| < 0.20$  GeV, and define a *signal* region of  $|M_{bc} - M_B| < 9$  MeV/ $c^2$  and  $|\Delta E| < 0.04$  GeV and two  $\Delta E$  *sideband* regions defined as  $-0.08$  GeV  $< \Delta E < -0.05$  GeV and  $0.05$  GeV  $< \Delta E < 0.15$  GeV [5]. The selection of sideband regions was based on a Monte Carlo study and was done in such a way that the relative fraction of  $B\bar{B}$  and  $q\bar{q}$  events match that of the signal region. For the normalization factor between the sideband and signal data samples we use the ratio of areas, namely 0.62.

To evaluate signal and background levels, we require that one of  $\Delta E$  or  $M_{bc}$  fall in its signal region and examine the distribution of candidates in the other, fitting to the sum of a signal distribution and an empirical background. The signal shapes in  $M_{bc}$  and  $\Delta E$  distributions are parameterized by a Gaussian and sum of two Gaussians with the same mean, respectively. The width of the  $M_{bc}$  distribution is primarily due to the c.m. energy spread and is expected to be the same for each channel; in the fit we fix it at the value  $\sigma_{M_{bc}} = 2.9$  MeV/ $c^2$  determined from the  $B^+ \rightarrow \bar{D}^0\pi^+$ ,  $\bar{D}^0 \rightarrow K^+\pi^-$  events in the same data sample. The  $\Delta E$  shape for the signal is also determined from the  $B^+ \rightarrow \bar{D}^0\pi^+$  events. For the  $M_{bc}$  projection, we parameterize the background with the empirical function  $f(M_{bc}) \propto \sqrt{1-x^2} \exp[-\xi(1-x^2)]$ , where  $x = M_{bc}/E_b$  and  $\xi$  is a parameter [6]. We fix the  $\xi$  value from a study of data below the  $B\bar{B}$  production threshold. We represent the  $\Delta E$  background shape with a linear function and restrict the fit to the range  $-0.1$  GeV  $< \Delta E < 0.2$  GeV [5].

### IV. BACKGROUND SUPPRESSION

An important issue for this analysis is the suppression of the large combinatoric background which is dominated by  $e^+e^- \rightarrow q\bar{q}$  continuum events. We suppress this background with variables that characterize the event topology.

Since the two  $B$  mesons produced from  $\Upsilon(4S)$  decay are nearly at rest in the c.m. frame, the angles of the decay products of the two  $B$ 's are uncorrelated and the events tend to be spherical. In contrast, hadrons from continuum  $q\bar{q}$  events tend to exhibit a two-jet structure. We use  $\theta_{\text{thr}}$ , which is the angle between the thrust axis of the  $B$  candidate and that of the rest of the event to discriminate between the two cases. The distribution of  $|\cos\theta_{\text{thr}}|$  is strongly peaked near  $|\cos\theta_{\text{thr}}| = 1.0$  for  $q\bar{q}$  events and is nearly flat for  $B\bar{B}$  events. We require  $|\cos\theta_{\text{thr}}| < 0.80$  for all three-body final states; this eliminates 83% of the continuum background and retains 79% of the signal events.

After imposing the  $\cos\theta_{\text{thr}}$  requirement, the remaining  $q\bar{q}$  and  $B\bar{B}$  events still have some differences in topology that are exploited for further continuum suppression. We divide the space around the  $B$  candidate thrust axis into nine polar angle intervals of  $10^\circ$  each; the  $i$ -th interval covers angles from  $(i-1)\times 10^\circ$  to  $i\times 10^\circ$ . We define the momentum flows,  $x_i$  ( $i = 1, 9$ ), into the  $i$ -th interval as a scalar sum of the momenta of all charged tracks and neutral showers directed in that interval. The momentum flows in corresponding forward and backward intervals are combined [7].

Angular momentum conservation provides some additional discrimination between  $B\bar{B}$  and continuum  $q\bar{q}$  events. In  $q\bar{q}$  production, the direction of the candidate thrust axis with respect to the beam axis in the c.m. frame,  $\theta_T$ , tends to reproduce the  $1 + \cos^2\theta_T$  distribution of the primary quarks. The direction of the  $B$  candidate thrust axis for  $B\bar{B}$  events is uniform. The  $B$  candidate direction with respect to the beam axis,  $\theta_B$ , exhibits a  $\sin^2\theta_B$  distribution for  $B\bar{B}$  events and is uniform for  $q\bar{q}$  events.

A Fisher discriminant [8] is formed from 11 variables: the nine momentum flow variables,  $|\cos\theta_T|$ , and  $|\cos\theta_B|$ . The discriminant,  $\mathcal{F}$ , is the linear combination

$$\mathcal{F} = \sum_{i=1}^{11} \alpha_i x_i$$

of the input variables,  $x_i$ , that maximizes the separation between signal and background. The coefficients  $\alpha_i$  are determined from Monte Carlo simulation using a large set of continuum events and signal events modeled as  $B^+ \rightarrow K^+\pi^+\pi^-$ . We use the same set of coefficients  $\alpha_i$  for all three-body final states. The separation between the mean values of the signal and background distributions is approximately 1.3 times the signal width.

For the  $K\pi\pi$  and  $KK\pi$  final states, we impose a requirement on the Fisher discriminant variable  $\mathcal{F}$  that rejects 90% of the remaining continuum background with about 54% efficiency for the signal. For the  $KKK$  final state, the continuum background is much smaller and we make a looser requirement that rejects 53% of continuum background with 89% efficiency for the signal.

To determine the dominant sources of background from other decay modes of  $B$  mesons, we use a large set of Monte Carlo generated  $B\bar{B}$  events where both  $B$  mesons decay generically [4]. Most of the  $B\bar{B}$  related background is found to originate from  $B^+ \rightarrow \bar{D}^0\pi^+$ ,  $B^+ \rightarrow J/\psi K^+$  and  $B^+ \rightarrow \psi(2S)K^+$  decays. To suppress this type of background we apply the requirements on the invariant masses of the two-particle combinations that are described below. The background from  $B$  semileptonic decays is additionally suppressed by the electron veto requirement. The most significant background to the  $K^+\pi^+\pi^-$  final state from rare  $B$  decays is found to originate from  $B^+ \rightarrow \eta'K^+$  followed by  $\eta' \rightarrow \pi^+\pi^-\gamma$ . We expect about 3% of these events to satisfy all the selection criteria. We find no significant background to the  $K^+K^+K^-$  final state from other known rare decays of  $B$  mesons.

## V. RESULTS OF THE ANALYSIS

### A. $B^+ \rightarrow K^+\pi^+\pi^-$

For  $B^+ \rightarrow K^+\pi^+\pi^-$  decays, we form  $B$  candidates from three charged tracks where one track is positively identified as a kaon and the other two tracks are consistent with a pion hypothesis. Figure 1 shows the Dalitz plot for selected  $B^+ \rightarrow K^+\pi^+\pi^-$  candidates in the  $B$  signal region. Large contributions from the  $B^+ \rightarrow \bar{D}^0\pi^+$ ,  $\bar{D}^0 \rightarrow K^+\pi^-$  and  $B^+ \rightarrow J/\psi(\psi(2S))K^+$ ,  $J/\psi(\psi(2S)) \rightarrow \mu^+\mu^-$  are apparent in the Dalitz plot. The  $J/\psi(\psi(2S))$  modes contribute to this final state due to muon-pion misidentification; the contribution from the  $J/\psi(\psi(2S)) \rightarrow e^+e^-$  submode is found to be negligible (less than 0.5%) after the electron veto requirement. For further analysis, we exclude  $\bar{D}^0$  and  $J/\psi(\psi(2S))$  signals by imposing requirements on the invariant masses of two intermediate particles:  $|M(K^+\pi^-) - M_D| > 0.10 \text{ GeV}/c^2$ ;  $|M(h^+h^-) - M_{J/\psi}| > 0.07 \text{ GeV}/c^2$ ;  $|M(h^+h^-) - M_{\psi(2S)}| > 0.05 \text{ GeV}/c^2$ , where  $h^+$  and  $h^-$  are pion candidates. For the  $J/\psi(\psi(2S))$  rejection, we use the muon mass hypothesis for charged tracks to calculate  $M(h^+h^-)$ . To suppress the background caused by  $\pi/K$  misidentification, we exclude candidates if the invariant mass of any pair of oppositely charged tracks from the  $B$  candidate is consistent with the  $D \rightarrow K\pi$  hypothesis within  $15 \text{ MeV}/c^2$  ( $\sim 2.5\sigma$ ), independently of the particle identification information ( $D$  veto). The  $\Delta E$  and  $M_{\text{bc}}$  distributions for the remaining events are presented in Figs. 2(a) and 2(b), respectively. Here a significant enhancement in the  $B$  signal region is observed; the result of a fit to the  $\Delta E$  distribution is presented in Table I. The expected  $\Delta E$  and  $M_{\text{bc}}$  background distributions, which are the sum of luminosity-scaled below-threshold data and generic  $B\bar{B}$  Monte Carlo events, are shown as open histograms in Figs. 2(a) and 2(b); the contributions from the  $B\bar{B}$  Monte Carlo sample are shown as hatched histograms. There are no three-body charmless decays included in the generic  $B\bar{B}$  Monte Carlo.

To examine possible intermediate two-body states in the observed  $B^+ \rightarrow K^+\pi^+\pi^-$  signal, we analyze the  $K^+\pi^-$  and  $\pi^+\pi^-$  invariant mass spectra shown in Fig. 3. To suppress the feed-across between the  $\pi^+\pi^-$  and  $K^+\pi^-$  states

we require the  $K^+\pi^-$  ( $\pi^+\pi^-$ ) invariant mass to be larger than 2.0 (1.5)  $\text{GeV}/c^2$  when making the  $\pi^+\pi^-$  ( $K^+\pi^-$ ) projection. The hatched histograms shown in Fig. 3 are the corresponding two-particle invariant mass spectra for the background events in the  $\Delta E$  sidebands plotted with a weight of 0.62.

The  $K^+\pi^-$  invariant mass spectrum is characterized by a narrow peak around 0.9  $\text{GeV}/c^2$  which is identified as the  $K^*(892)^0$  and a broad enhancement above 1.0  $\text{GeV}/c^2$  which is subsequently referred to as  $K_X(1400)$ . In the  $\pi^+\pi^-$  invariant mass spectrum two distinct structures in the low mass region are observed. One is slightly below 1.0  $\text{GeV}/c^2$  and is identified as the  $f_0(980)$  while the other is between 1.0  $\text{GeV}/c^2$  and 1.5  $\text{GeV}/c^2$  and is referred to as  $f_X(1300)$ . Some excess of signal events can be also observed in the  $\rho^0(770)$  mass region. The peak around 3.4  $\text{GeV}/c^2$  is consistent with the process  $B^+ \rightarrow \chi_{c0}K^+$ ,  $\chi_{c0} \rightarrow \pi^+\pi^-$ , and is the subject of a separate analysis [9]. In this paper we exclude the  $B^+ \rightarrow \chi_{c0}K^+$  candidates from the analysis of two-body final states by applying the requirement on the  $\pi^+\pi^-$  invariant mass:  $|M(\pi^+\pi^-) - M_{\chi_{c0}}| > 0.05 \text{ GeV}/c^2$ .

For further analysis we subdivide the full Dalitz plot area into seven non-overlapping regions as defined in Table II. Regions from I to V are arranged to contain the major part of the signal from the  $B^+ \rightarrow K^*(892)^0\pi^+$ ,  $B^+ \rightarrow K_X(1400)\pi^+$ ,  $B^+ \rightarrow \rho^0(770)K^+$ ,  $B^+ \rightarrow f_0(980)K^+$ , and  $B^+ \rightarrow f_X(1300)K^+$  final states, respectively. The area in the Dalitz plot where  $K\pi$  and  $\pi\pi$  resonances overlap is covered by region VI, and region VII covers the rest of the Dalitz plot. The results of the fits to the  $\Delta E$  distributions for all seven regions are summarized in Table II. The procedure used for the extraction of the two-body branching fractions is described in detail in Section VI.

### B. $B^+ \rightarrow K^+K^+K^-$

For the selection of  $B^+ \rightarrow K^+K^+K^-$  events, we use combinations of three charged tracks that are positively identified as kaons. The Dalitz plot for selected  $B^+ \rightarrow K^+K^+K^-$  candidate events in the  $B$  signal region after the  $D$  veto is shown in Fig. 4. Since in this case there are two same-charge kaons, we distinguish the  $K^+K^-$  combinations with smaller,  $M(K^+K^-)_{\min}$ , and larger,  $M(K^+K^-)_{\max}$ , invariant masses. We avoid double entries per candidate by forming the Dalitz plot as  $M^2(K^+K^-)_{\max}$  versus  $M^2(K^+K^-)_{\min}$ . The signal from the Cabibbo-suppressed  $B^+ \rightarrow \bar{D}^0K^+$ ,  $\bar{D}^0 \rightarrow K^+K^-$  decay mode is apparent as a vertical strip in the Dalitz plot. The corresponding Cabibbo-allowed  $B^+ \rightarrow \bar{D}^0\pi^+$ ,  $\bar{D}^0 \rightarrow K^+K^-$  decays can also contribute to this final state as a result of pion-kaon misidentification. We exclude candidates consistent with the  $B^+ \rightarrow \bar{D}^0h^+$  hypothesis from further analysis by imposing the requirement on the  $K^+K^-$  invariant mass  $|M(K^+K^-) - M_{D^0}| > 0.025 \text{ GeV}/c^2$ . The  $\Delta E$  and  $M_{bc}$  distributions after the exclusion of  $D$  mesons are presented in Figs. 2(c) and 2(d) respectively. A large peak in the  $B$  signal region is apparent in both distributions. The result of a fit to the  $\Delta E$  distribution is presented in Table I.

The  $K^+K^-$  invariant mass spectra for events from the  $B$  signal region are shown as open histograms in Figs. 5(a)-5(c). The hatched histograms show the corresponding spectra for background events in the  $\Delta E$  sidebands, plotted with a weight of 0.62. The  $M(K^+K^-)_{\min}$  spectrum, shown in Fig. 5(a), is characterized by a narrow peak at 1.02  $\text{GeV}/c^2$  corresponding to the  $\phi(1020)$  meson and a broad structure around 1.5  $\text{GeV}/c^2$ ; this is subsequently referred to as  $f_X(1500)$ . To plot the  $M(K^+K^-)_{\max}$  mass spectrum we subdivide the  $M(K^+K^-)_{\min}$  mass region into two ranges:  $M(K^+K^-)_{\min} < 1.1 \text{ GeV}/c^2$  and  $M(K^+K^-)_{\min} > 1.1 \text{ GeV}/c^2$ . The  $M(K^+K^-)_{\max}$  mass spectra for these two regions are presented in Fig. 5(b) and Fig. 5(c) respectively. The prominent structure observed in Fig. 5(b) reflects the 100%  $\phi$  meson polarization in the  $B^+ \rightarrow \phi K^+$  decay due to angular momentum conservation. In contrast, the distribution of signal events in Fig. 5(c) is quite uniform after the background is subtracted. For the analysis of two-body final states we exclude events that are consistent with the  $B^+ \rightarrow \chi_{c0}K^+$ ,  $\chi_{c0} \rightarrow K^+K^-$  decay by applying the requirement on the  $K^+K^-$  invariant mass:  $|M(K^+K^-) - M_{\chi_{c0}}| > 0.05 \text{ GeV}/c^2$ .

For further analysis we subdivide the full Dalitz plot area into the four non-overlapping regions defined in Table III. Regions I and II are arranged to contain the major part of the signal from the  $B^+ \rightarrow \phi(1020)K^+$  and  $B^+ \rightarrow f_X(1500)K^+$  final states, respectively. Regions III and IV cover the remaining part of the Dalitz plot. The results of the fits to the  $\Delta E$  distributions for all four regions are summarized in Table III.

### C. $B^+ \rightarrow K^-\pi^+\pi^+$ , $B^+ \rightarrow K^+K^+\pi^-$ and $B^+ \rightarrow K^+K^-\pi^+$

In general, we do not expect any signal in the  $B^+ \rightarrow K^-\pi^+\pi^+$  and  $B^+ \rightarrow K^+K^+\pi^-$  final states. The Standard Model prediction for the  $B^+ \rightarrow K^+K^+\pi^-$  branching fraction is of the order of  $10^{-11}$ , and even much smaller for the  $B^+ \rightarrow K^-\pi^+\pi^+$  final state [11]. However, these signals could be significantly enhanced in some extensions of the Standard Model [12], and, thus, these modes can be used to search for physics beyond the Standard Model.

For the  $K^+K^+\pi^-$  final state, we reject candidates that are consistent with the  $B^+ \rightarrow \bar{D}^0K^+$ ,  $\bar{D}^0 \rightarrow K^+\pi^-$  decay by imposing the requirement on the  $K^+\pi^-$  invariant mass  $|M(K^+\pi^-) - M_{D^0}| > 0.10 \text{ GeV}/c^2$ . In case of the  $K^+K^-\pi^+$  channel we reject candidates that are consistent with the  $B^+ \rightarrow \bar{D}^0\pi^+$ ,  $\bar{D}^0 \rightarrow K^+K^-$  decay with the requirement

$|M(K^+K^-) - M_{D^0}| > 0.05 \text{ GeV}/c^2$ . We also apply the  $D$  veto requirement for the three modes. The resulting  $\Delta E$  and  $M_{bc}$  distributions for the  $K^-\pi^+\pi^+$ ,  $K^+K^+\pi^-$  and  $K^+K^-\pi^+$  final states are presented in Figs. 2(e)-2(j). Although we do not observe any signal in the  $\Delta E$  distributions, there is an excess of events in the signal region of the  $M_{bc}$  distributions for the  $K^-\pi^+\pi^+$  and  $K^+K^-\pi^+$  final states. These excesses could be caused by incorrectly reconstructed  $B$  decays. To subtract this background we subdivide the  $\Delta E$  region into ten bins of 40 MeV width and determine the signal yield in each bin from the fit to the corresponding  $M_{bc}$  spectrum. The results of the fit, along with the expected contributions from the generic  $B\bar{B}$  decays and the feed-down due to the particle misidentification from the  $B^+ \rightarrow K^+\pi^+\pi^-$  and  $B^+ \rightarrow K^+K^+K^-$  decay modes, are presented in Fig. 6. The latter two components are shown in Fig. 6 by the dotted and dashed histograms, respectively. The excess of events over the total expected background in the  $\Delta E$  signal region (two bins around  $\Delta E = 0$ ) is considered to be a signal yield. The results are summarized in Table I. We do not observe a statistically significant signal in any of these three-body modes.

The feed-across between  $K^+\pi^+\pi^-$  and  $K^+K^+K^-$  final states is found to be negligible. True  $B^+ \rightarrow K^+K^+K^-$  events reconstructed as  $K^+\pi^+\pi^-$  contribute mainly to the  $\Delta E < -0.10 \text{ GeV}$  region that is excluded from the fit. The fraction of true  $K^+\pi^+\pi^-$  events improperly reconstructed as  $K^+K^+K^-$  is less than 0.1%.

## VI. BRANCHING FRACTIONS

To determine branching fractions, we normalize our results to the observed  $B^+ \rightarrow \bar{D}^0\pi^+$ ,  $\bar{D}^0 \rightarrow K^+\pi^-$  signal. This removes systematic effects in the particle identification efficiency, charged track reconstruction efficiency and the systematic uncertainty due to the cuts on event shape variables. We calculate the branching fraction for  $B$  meson decay to a particular final state  $f$  via the relation

$$\mathcal{B}(B^+ \rightarrow f) = \mathcal{B}(B^+ \rightarrow \bar{D}^0\pi^+)\mathcal{B}(\bar{D}^0 \rightarrow K^+\pi^-)\frac{N_f}{N_{D\pi}}\frac{\varepsilon_{D\pi}}{\varepsilon_f},$$

where  $N_f$  and  $N_{D\pi}$  are the numbers of reconstructed events for the final state  $f$  and that for the reference process, respectively;  $\varepsilon_f$  and  $\varepsilon_{D\pi}$  are the corresponding reconstruction efficiencies. We use the signal yield extracted from the fit to the corresponding  $\Delta E$  distribution; we do not use the  $M_{bc}$  distribution, because it, in general, suffers more from the  $B\bar{B}$  background.

The number of signal events for the reference process  $B^+ \rightarrow \bar{D}^0\pi^+$ ,  $\bar{D}^0 \rightarrow K^+\pi^-$  is found to be  $1349 \pm 40$  for the  $K^+K^+K^-$  selection requirements and  $805 \pm 32$  for the requirements used for all other three-body combinations. The corresponding reconstruction efficiencies are 26.8% and 16.1%, respectively. The reconstruction efficiency for each three-body final state is determined from the Monte Carlo simulation of events that are generated with a uniform Dalitz plot distribution. The branching fraction results for  $K^+\pi^+\pi^-$  and  $K^+K^+K^-$  final states are presented in Table I, where the first quoted error is statistical and the second is systematic. The dominant sources of systematic error are listed in Table IV. We estimate the systematic uncertainty due to variations of reconstruction efficiency over the Dalitz plot using two sets of MC data generated with uniform distribution (phase space) and using some model (described below). The uncertainty due to the particle identification is estimated using pure samples of kaons and pions from  $D^0 \rightarrow K^+\pi^-$  decays, where the  $D^0$  flavor is tagged using  $D^{*+} \rightarrow D^0\pi^+$  decays. To estimate the uncertainty due to the signal and background shapes parameterization, we fit the  $\Delta E$  distributions using different functions for the background description (linear, parabolic, exponential plus constant) and varying the parameters of the signal function (sum of two Gaussians with the same mean) within their errors.

Since we do not observe a statistically significant signal in the  $K^-\pi^+\pi^+$ ,  $K^+K^+\pi^-$  or  $K^+K^-\pi^+$  final states, we place the 90% confidence level upper limits on their branching fractions. These limits are given in Table I. To calculate the upper limits, we follow the PDG recommendation [13].

### A. Exclusive two-body branching fractions in the $K^+\pi^+\pi^-$ final state

In the determination of the branching fractions for exclusive two-body final states, we have to take into account the possibility of interference between wide resonances. This requires some assumptions about the states that are being observed and, as a consequence, introduces some model dependence into the extraction of the exclusive branching fractions. The present level of statistics does not permit unambiguous interpretation of the  $K_X(1400)$  and  $f_X(1300)$  states and, thus, it is not possible to use the data to fix all of the input model parameters. For this analysis we assume that the observed  $K_X(1400)$  and  $f_X(1300)$  states are  $0^+$  scalars. While this does not contradict the observed signal, some contributions from vector ( $1^-$ ) and tensor ( $2^+$ ) resonances cannot be excluded. The uncertainty related to this assumption is included in the model-dependent error described below. We ascribe to the  $K_X(1400)$  state the

parameters of  $K_0^*(1430)$  ( $M = 1412$  MeV/ $c^2$ ,  $\Gamma = 294$  MeV) and to  $f_X(1300)$  state the parameters of  $f_0(1370)$  ( $M = 1370$  MeV/ $c^2$ ,  $\Gamma = 400$  MeV) [10].

For further analysis we make the following assumptions:

- The observed signal in the  $K^+\pi^+\pi^-$  final state can be described by some number of two-body final states. We restrict ourselves to the following set of exclusive two-body final states:  $K^*(892)^0\pi^+$ ,  $K_X(1400)\pi^+$ ,  $\rho^0(770)K^+$ ,  $f_0(980)K^+$  and  $f_X(1300)K^+$ . We enumerate these final states as 1 through 5 in the order mentioned above.
- Given this set of two-body final states, we determine the exclusive branching fractions neglecting the effects of interference. The uncertainty due to possible interference between different intermediate states is included in the final result as a model-dependent error.

In order to extract the signal yield for each two-body final state, we perform a simultaneous likelihood fit to the  $\Delta E$  distributions for the seven regions of the  $K^+\pi^+\pi^-$  Dalitz plot. We express the expected number  $n_j$  of signal events in the  $j$ -th region of the Dalitz plot as a linear combination

$$n_j = \sum_{i=1}^5 \varepsilon_{ij} N_i,$$

where  $N_i$  is the total number of signal events in the  $i$ -th two-body final state and  $\varepsilon_{ij}$  is the probability for the  $i$ -th final state to contribute to the  $j$ -th region in the Dalitz plot. The  $\varepsilon_{ij}$  matrix is determined from the Monte Carlo simulation and includes the reconstruction efficiency. This procedure takes into account the effect of correlations between different channels in the determination of the statistical errors.

The results of the fit are summarized in Table V. Combining all the relevant numbers, we calculate the product of branching fractions  $\mathcal{B}(B^+ \rightarrow Rh^+) \times \mathcal{B}(R \rightarrow h^+h^-)$ , where  $R$  denotes the two-body intermediate resonant state. We present three types of errors for the branching fractions: the first error is statistical, the second is systematic, and the third reflects the model-dependent uncertainty. In general, the model-dependent error is due to uncertainties in the effects of interference between different resonant states. We estimate this error by means of a  $B^+ \rightarrow K^+\pi^+\pi^-$  Monte Carlo simulation that includes interference effects between all the final states mentioned above. We vary the relative phases of the resonances and determine the signal yield using the procedure described above. The maximal deviations from the central values are used as an estimate of the model dependence of the obtained branching fractions. We find that the model-dependent errors associated with the wide resonances introduce significant uncertainties into the branching fraction determination. In the case of the  $\rho^0(770)K^+$  final state, this effect is enhanced by the smallness of the signal itself. Since we do not observe a significant signal in this channel, we report a 90% confidence level upper limit. The statistical significance of the signal, in terms of the number of standard deviations, is calculated as  $\sqrt{-2 \ln(\mathcal{L}_0/\mathcal{L}_{\max})}$ , where  $\mathcal{L}_{\max}$  and  $\mathcal{L}_0$  denote the maximum likelihood with the nominal signal yield and with the signal yield fixed at zero, respectively.

## B. Exclusive two-body branching fractions in the $K^+K^+K^-$ final state

In the case of the three charged kaon final state, we clearly observe the  $\phi(1020)$  meson plus a very broad  $f_X(1500)$  structure that we currently cannot interpret unambiguously. It could be a complex superposition of several intermediate states and some contribution from the non-resonant  $B^+ \rightarrow K^+K^+K^-$  decay is also possible. For our study of systematic and model-dependent uncertainties, we construct a simplified model and parameterize the  $f_X(1500)$  structure as a hypothetical scalar state with  $M = 1500$  MeV/ $c^2$  and  $\Gamma = 700$  MeV. We find qualitative agreement between the experimental Dalitz plot distribution of the signal events and that obtained from the Monte Carlo simulation with this simple model.

Then we extract the signal yield for the two-body final states:  $B^+ \rightarrow \phi(1020)K^+$  and the so-called  $B^+ \rightarrow f_X(1500)K^+$ , which is, in fact, all of the remaining signal. We follow the same procedure as we used for the  $K^+\pi^+\pi^-$  final state. The signal yields are determined from a simultaneous fit to the  $\Delta E$  distributions for four separate regions of the  $K^+K^+K^-$  Dalitz plot. The results of the fit are summarized in Table VI.

We determine the model-dependent error in the same way as we did for the  $K^+\pi^+\pi^-$  final state. In the case of the  $K^+K^+K^-$  final state the model-dependent error is found to be much smaller than in the  $K^+\pi^+\pi^-$  final state. This is mainly due to the small width of the  $\phi(1020)$  meson.

## VII. DISCUSSION & CONCLUSION

The high quality of  $\pi/K$  separation at Belle allows us to measure, for the first time, the branching ratios for the three-body modes  $\mathcal{B}(B^+ \rightarrow K^+\pi^-\pi^+) = (55.6 \pm 5.8 \pm 7.7) \times 10^{-6}$  and  $\mathcal{B}(B^+ \rightarrow K^+K^-K^+) = (35.3 \pm 3.7 \pm 4.5) \times 10^{-6}$  without assumptions about particular intermediate mechanisms. CLEO [14] and BaBar [15] have previously placed upper limits on the branching fractions of non-resonant three-body decays:  $\mathcal{B}(B^+ \rightarrow K^+\pi^+\pi^-) < 28 \times 10^{-6}$  (CLEO),  $\mathcal{B}(B^+ \rightarrow K^+\pi^+\pi^-) < 66 \times 10^{-6}$  (BaBar),  $\mathcal{B}(B^+ \rightarrow K^+K^+K^-) < 38 \times 10^{-6}$  (CLEO). A comparison of the applied selection criteria shows that CLEO and BaBar restricted their analyses to the region of invariant mass above 2 GeV/ $c^2$  for any pair of the particles. This requirement effectively removes most of the low mass resonances that provide the dominant contribution to our observed signal. They assume a uniform distribution of events over the Dalitz plot to obtain the limits quoted above. The upper limits reported here for the  $K^-\pi^+\pi^+$ ,  $K^+K^+\pi^-$  and  $K^+K^-\pi^+$  modes are considerably more restrictive than previous limits from CLEO [14] and OPAL [16].

Significant signals are observed for the first time in the decay modes  $B^+ \rightarrow f_0(980)K^+$  and  $B^+ \rightarrow K^*(892)^0\pi^+$ . The measured branching fraction product for the  $f_0(980)K^+$  final state is  $\mathcal{B}(B^+ \rightarrow f_0(980)K^+) \times \mathcal{B}(f_0(980) \rightarrow \pi^+\pi^-) = (9.6_{-2.3-1.5-0.8}^{+2.5+1.5+3.4}) \times 10^{-6}$ . This is the first observation of a  $B$  decay to a charmless scalar-pseudoscalar final state. The measured branching fraction product for the  $K^*(892)^0\pi^+$  final state is  $\mathcal{B}(B^+ \rightarrow K^*(892)^0\pi^+) \times \mathcal{B}(K^*(892)^0 \rightarrow K^+\pi^-) = (12.9_{-2.6-1.4-4.5}^{+2.8+1.4+2.3}) \times 10^{-6}$ . Using the value of  $\mathcal{B}(K^*(892)^0 \rightarrow K^+\pi^-) = 2/3$ , we translate our measurement into the branching fraction  $\mathcal{B}(B^+ \rightarrow K^*(892)^0\pi^+) = (19.4_{-3.9-2.1-6.8}^{+4.2+2.1+3.5}) \times 10^{-6}$ . The significant enhancement in the  $K^+\pi^-$  invariant mass spectrum above the  $K^*(892)$  mass agrees with the scalar  $K_0^*(1430)$  hypothesis. This is also in agreement with theoretical predictions [17] for the  $B^+ \rightarrow K_0^*(1430)\pi^+$  branching fraction based on the factorization model. Nevertheless, we cannot exclude some contribution from the tensor  $K_2^*(1430)$  state.

The interpretation of the peak with a  $\pi^+\pi^-$  invariant mass around 1300 MeV/ $c^2$  in the  $K^+\pi^+\pi^-$  system is less certain. There are two known candidate states: the  $f_2(1270)$  and  $f_0(1370)$  [10]. Attributing the peak to the  $f_0(1370)$ , with its rather small coupling to  $\pi^+\pi^-$  [18], would lead to an unusually large branching fraction for a charmless  $B$  decay mode. On the other hand, as recently shown in [19], the factorization model predicts a very small branching fraction for the  $B^+ \rightarrow f_2(1270)K^+$ . If our observation is, in fact, due to the  $f_2(1270)$ , this would provide evidence for a significant nonfactorizable contribution.

We cannot identify the broad structure observed in the  $B^+ \rightarrow K^+K^+K^-$  final state above the  $\phi(1020)$  meson. It is hardly compatible with the presence of a single scalar state, either  $f_0(1370)$  or  $f_0(1500)$  [10]. We also cannot exclude the presence of a non-resonant contribution or the case of several resonances contributing to the excess in the  $K^+K^-$  invariant mass spectrum seen around 1.5 GeV/ $c^2$ .

We find that effects of interference between different two-body intermediate states can have significant influence on the observed two-particle mass spectra and a full amplitude analysis of three-body  $B$  meson decays is required for a more complete understanding. This will be possible with increased statistics.

### Acknowledgement

We wish to thank the KEKB accelerator group for the excellent operation of the KEKB accelerator. We acknowledge support from the Ministry of Education, Culture, Sports, Science, and Technology of Japan and the Japan Society for the Promotion of Science; the Australian Research Council and the Australian Department of Industry, Science and Resources; the Department of Science and Technology of India; the BK21 program of the Ministry of Education of Korea and the CHEP SRC program of the Korea Science and Engineering Foundation; the Polish State Committee for Scientific Research under contract No.2P03B 17017; the Ministry of Science and Technology of Russian Federation; the National Science Council and the Ministry of Education of Taiwan; and the U.S. Department of Energy.

- 
- [1] R. Godang *et al.* (CLEO Collaboration), Phys. Rev. Lett. **80**, 3456 (1998).  
D. Cronin-Hennessy *et al.* (CLEO Collaboration), Phys. Rev. Lett. **85**, 515 (2000).  
C.P. Jessop *et al.* (CLEO Collaboration), Phys. Rev. Lett. **85**, 2881 (2000).
- [2] KEKB B Factory Design Report, KEK Report 95-7 (1995), unpublished; Y. Funakoshi *et al.*, Proc. 2000 European Particle Accelerator Conference, Vienna (2000).
- [3] A. Abashian *et al.* (Belle Collaboration), KEK Progress Report 2000-4 (2000), to appear in Nucl. Inst. and Meth. A.
- [4] Events are generated with the CLEO group's QQ program (<http://www.lns.cornell.edu/public/CLEO/soft/qq>); the detector response is simulated using GEANT, R.Brun *et al.*, GEANT 3.21, CERN Report DD/EE/84-1, 1984.



- [5] The negative  $\Delta E$  region could contain events from  $B \rightarrow Khh\pi$  with an additional low momentum neutral or charged pion that is not included in the  $M_{bc}$  and  $\Delta E$  computation. Therefore, we do not use the  $\Delta E < -0.1$  GeV region for sideband studies and also exclude it from the fits.
- [6] H. Albrecht *et al.* (ARGUS Collaboration), Phys. Lett. B **229**, 304 (1989).
- [7] D.M. Asner *et al.* (CLEO Collaboration), Phys. Rev. D **53**, 1039 (1996).
- [8] R.A. Fisher, Ann. Eugenics **7**, 179 (1936);  
M.G. Kendall and A. Stuart, *The Advanced Theory of Statistics*, 2nd ed. (Hafner Publishing, New York, 1968), Vol. III.
- [9] K. Abe *et al.* (Belle Collaboration), Phys. Rev. Lett. **88**, 031802 (2002).
- [10] D.E. Groom *et al.* (Particle Data Group), Eur. Phys. J. C **15**, 1 (2000).
- [11] K. Huitu, C.D. Lu, P. Singer, D.X. Zhang, Phys. Rev. Lett. **81**, 4313 (1998).
- [12] K. Huitu, C.D. Lu, P. Singer, D.X. Zhang, Phys. Lett. **B** 445, 394 (1999);  
S. Fajfer and P. Singer, Phys. Rev. **D** 62, 117702 (2000);  
S. Fajfer and P. Singer, Phys. Rev. **D** 65, 017301 (2002).
- [13] G.J. Feldman and R.D. Cousins, Phys. Rev. D **57**, 3873 (1998).
- [14] T. Bergfeld *et al.* (CLEO Collaboration), Phys. Rev. Lett. **77**, 4503 (1996).
- [15] T.J. Champion (BaBar Collaboration), Proc. of the XXX-th Int. Conf. on High Energy Phys., Osaka (2000).
- [16] G. Abbiendi *et al.* (OPAL Collaboration), Phys. Lett. B **476**, 233 (2000).
- [17] V.L. Chernyak, Phys. Lett. B **509**, 273 (2001). In this work the branching fraction is calculated using  $f_{K^*} = (70 \pm 10)$  MeV obtained from light cone sum rules. Other estimates of  $f_{K^*}$  exist in literature, e.g. the value 42 MeV has been suggested by K. Maltman, Phys. Lett. B **462**, 14 (1999).
- [18] V.V. Anisovich, V.A. Nikonov, A.V. Sarantsev, hep-ph/0102338, 2001.
- [19] C.S. Kim, B.H. Lim, S. Oh, Eur. Phys. J. **C22**, 683 (2002).

TABLE I: Branching fractions and 90% C.L. upper limits for  $B^+ \rightarrow K^+ h^+ h^-$  final states.

Three-body mode	Efficiency (%)	Yield (events)	$\mathcal{B}$ ( $10^{-6}$ )
$K^+ \pi^+ \pi^-$	17.3	$237 \pm 23$	$55.6 \pm 5.8 \pm 7.7$
$K^+ K^+ K^-$	24.0	$210 \pm 21$	$35.3 \pm 3.7 \pm 4.5$
$K^- \pi^+ \pi^+$	16.2	$12 \pm 9$	$< 7.0$
$K^+ K^+ \pi^-$	14.2	$2.0 \pm 5.3$	$< 3.2$
$K^+ K^- \pi^+$	14.6	$26 \pm 12$	$< 12$

TABLE II: Results of the fit to the  $\Delta E$  distribution for different regions in the  $K^+ \pi^+ \pi^-$  Dalitz plot. Columns list the definition of each region, reconstruction efficiency from Monte Carlo simulation and signal yield.

Dalitz plot region	Mass range ( $\text{GeV}/c^2$ )	Efficiency (%)	Yield (events)
I	$M(K\pi) < 1.00; M(\pi\pi) > 1.50$	$20.7 \pm 3.7$	$47.1^{+9.3}_{-8.7}$
II	$1.00 < M(K\pi) < 2.00; M(\pi\pi) > 1.50$	$19.2 \pm 1.3$	$56.0^{+12}_{-11}$
III	$M(\pi\pi) < 0.90; M(K\pi) > 2.00$	$16.7 \pm 2.4$	$17.7^{+8.4}_{-7.8}$
IV	$0.90 < M(\pi\pi) < 1.06; M(K\pi) > 2.00$	$19.9 \pm 3.2$	$34.7^{+7.9}_{-7.3}$
V	$1.06 < M(\pi\pi) < 1.50; M(K\pi) > 2.00$	$19.6 \pm 1.7$	$33.4^{+8.8}_{-8.2}$
VI	$M(K\pi) < 2.00; M(\pi\pi) < 1.50$	$14.7 \pm 3.3$	$14.9^{+6.3}_{-5.7}$
VII	$M(K\pi) > 2.00; M(\pi\pi) > 1.50$	$16.1 \pm 0.5$	$11.8^{+9.4}_{-8.8}$

TABLE III: Results of the fit to the  $\Delta E$  distribution for different regions in the  $K^+ K^+ K^-$  Dalitz plot. Columns list the definition of each region, reconstruction efficiency from Monte Carlo simulation and signal yield.

Dalitz plot region	Mass range ( $\text{GeV}/c^2$ )	Efficiency (%)	Yield (events)
I	$M(KK)_{\min} < 1.04$	$24.6 \pm 2.5$	$35.7^{+7.1}_{-6.5}$
II	$1.04 < M(KK)_{\min} < 2.00$	$23.3 \pm 0.8$	$113^{+15}_{-14}$
III	$M(KK)_{\min} > 2.00; M(KK)_{\max} > 3.40$	$23.9 \pm 1.1$	$14.7^{+7.0}_{-6.4}$
IV	$M(KK)_{\min} > 2.00; M(KK)_{\max} < 3.40$	$24.7 \pm 0.8$	$32.3^{+6.8}_{-6.1}$

TABLE IV: List of systematic errors (in percent) for the  $B^+ \rightarrow K^+ h^+ h^-$  branching fractions.

Source	$K^+ \pi^+ \pi^-$	$K^- \pi^+ \pi^+$	$K^+ K^- \pi^+$	$K^+ K^+ \pi^-$	$K^+ K^+ K^-$
$B \rightarrow D\pi$ and $D \rightarrow K\pi$ branching fractions	9.7	9.7	9.7	9.7	9.7
efficiency nonuniformity over the Dalitz plot	7.6	-	-	-	3.7
background and signal parameterization	6.3	-	-	-	4.7
particle identification	-	-	3.0	3.0	6.0
total	13.8	9.7	10.1	10.1	12.9

TABLE V: Results of the simultaneous fit to the  $K^+\pi^+\pi^-$  final state.

Two-body mode	Efficiency (%)	Yield (events)	Significance ( $\sigma$ )	$\mathcal{B}_{B^+\rightarrow Rh^+} \times \mathcal{B}_{R\rightarrow h^+h^-}$ ( $10^{-6}$ )
$K^*(892)^0\pi^+$	18.9	$60^{+13}_{-12}$	6.2	$12.9^{+2.8+1.4+2.3}_{-2.6-1.4-4.5}$
$K_X(1400)\pi^+$	16.2	$58^{+14}_{-13}$	4.9	$14.5^{+3.5+1.8+3.3}_{-3.3-1.8-6.5}$
$\rho^0(770)K^+$	15.1	$9^{+13}_{-12}$	0.8	< 12
$f_0(980)K^+$	17.8	$42^{+11}_{-10}$	5.0	$9.6^{+2.5+1.5+3.4}_{-2.3-1.5-0.8}$
$f_X(1300)K^+$	16.9	$46^{+14}_{-13}$	3.9	$11.1^{+3.4+1.4+7.2}_{-3.1-1.4-2.9}$

TABLE VI: Results of the simultaneous fit to the  $K^+K^+K^-$  final state.

Two-body mode	Efficiency (%)	Yield (events)	Significance ( $\sigma$ )	$\mathcal{B}_{B^+\rightarrow Rh^+} \times \mathcal{B}_{R\rightarrow h^+h^-}$ ( $10^{-6}$ )
$\phi(1020)K^+$	23.6	$42^{+8.7}_{-7.9}$	7.2	$7.2^{+1.5+0.9+0.4}_{-1.4-0.9-0.4}$
$f_X(1500)K^+$	21.3	$146^{+17}_{-17}$	12	$27.6^{+3.2+3.5+1.4}_{-3.2-3.5-1.4}$

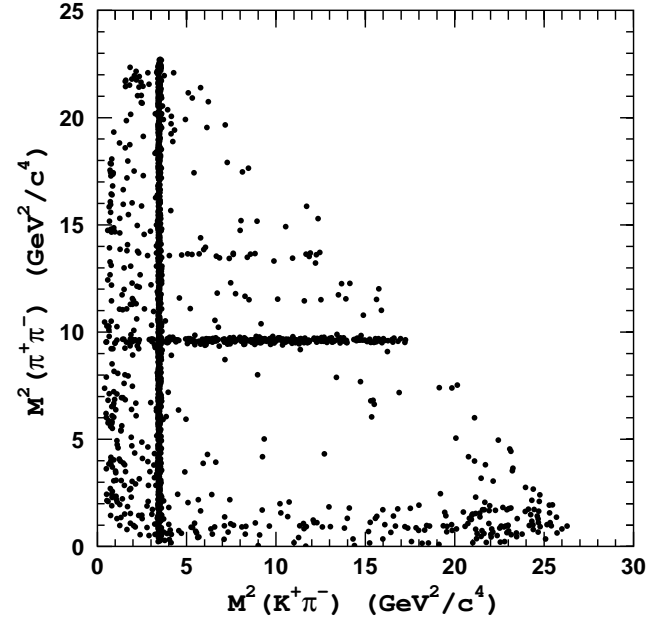


FIG. 1: The Dalitz plot for  $B^+ \rightarrow K^+ \pi^+ \pi^-$  candidates from the  $B$  signal region.

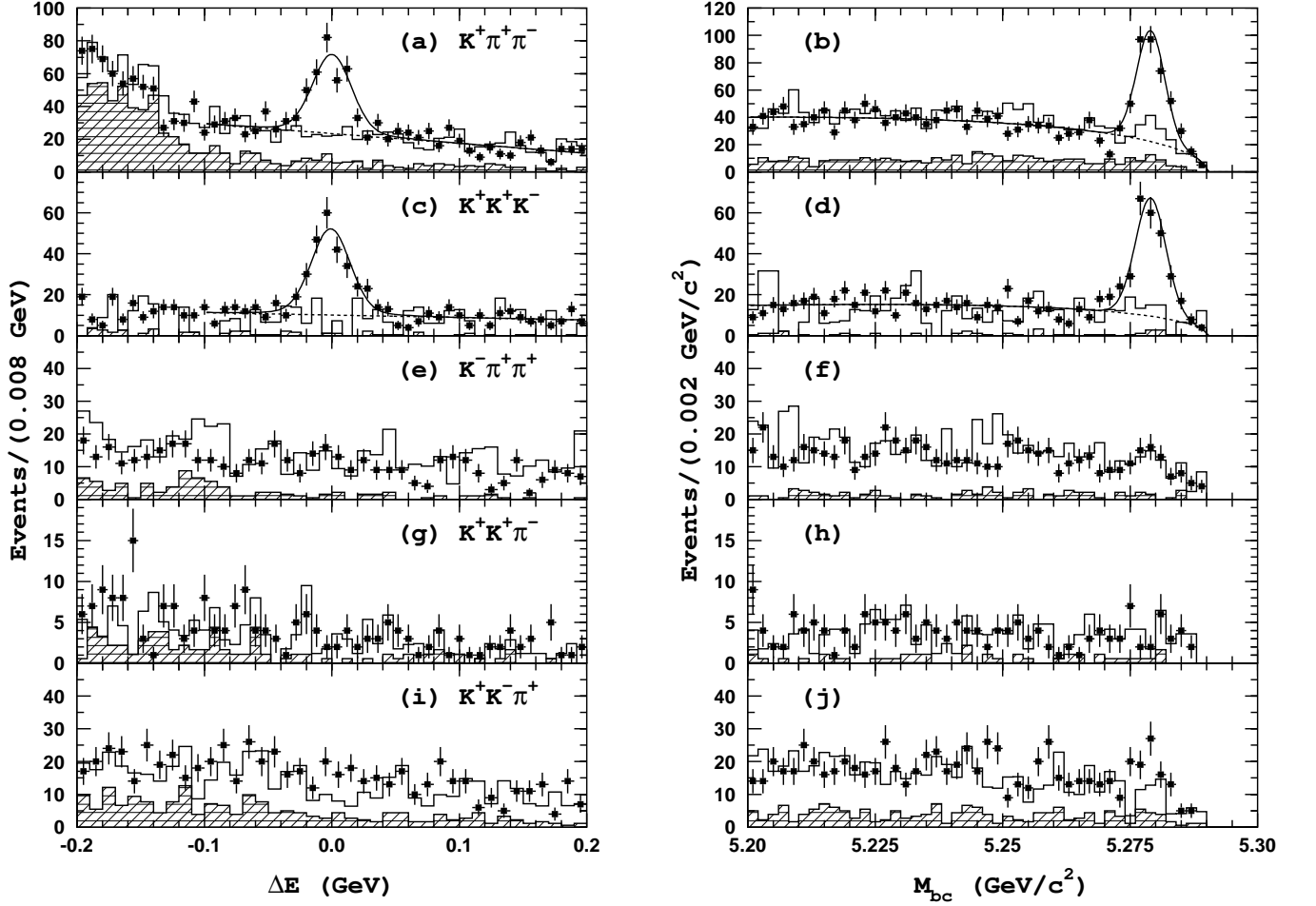


FIG. 2: The  $\Delta E$  (left) and  $M_{bc}$  (right) distributions for  $B^+ \rightarrow K^+ h^+ h^-$  final states: (a, b) -  $K^+ \pi^+ \pi^-$ ; (c, d) -  $K^+ K^+ K^-$ ; (e, f) -  $K^- \pi^+ \pi^+$ ; (g, h) -  $K^+ K^+ \pi^-$ ; (i, j) -  $K^+ K^- \pi^+$ . Points with errors represent data, open histograms are the proper sum of the below-threshold data and  $B\bar{B}$  Monte Carlo; the hatched histograms show the contribution of  $B\bar{B}$  Monte Carlo only. The solid lines display the signal plus background combined shape. The dashed lines correspond to the background shape only.

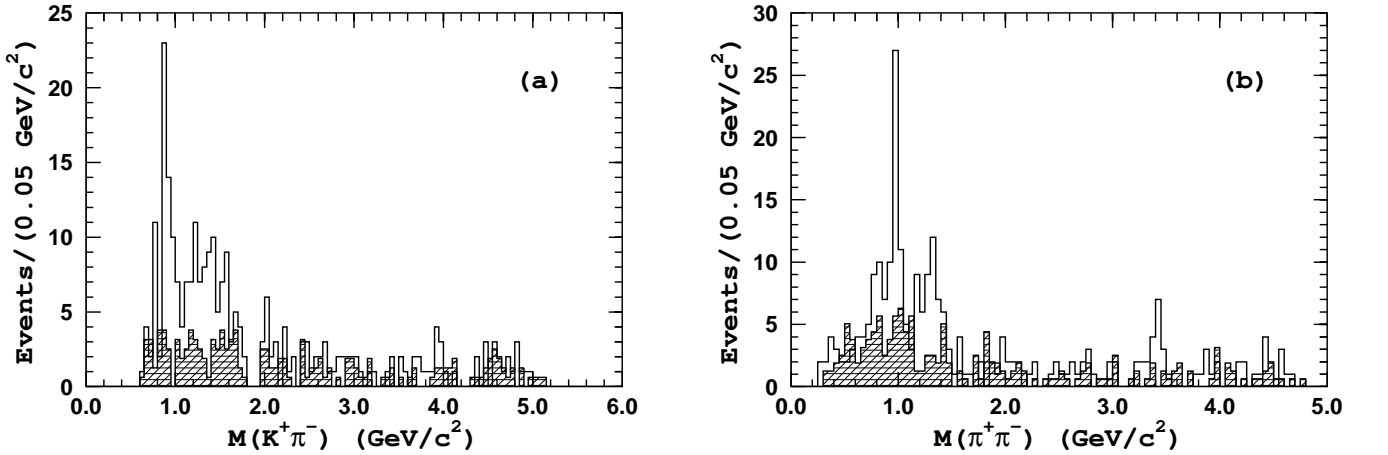


FIG. 3: The (a)  $K^+ \pi^-$  and (b)  $\pi^+ \pi^-$  invariant mass spectra for selected  $B^+ \rightarrow K^+ \pi^+ \pi^-$  candidates in the  $B$  signal region (open histograms) and for background events in the  $\Delta E$  sidebands (hatched histograms).

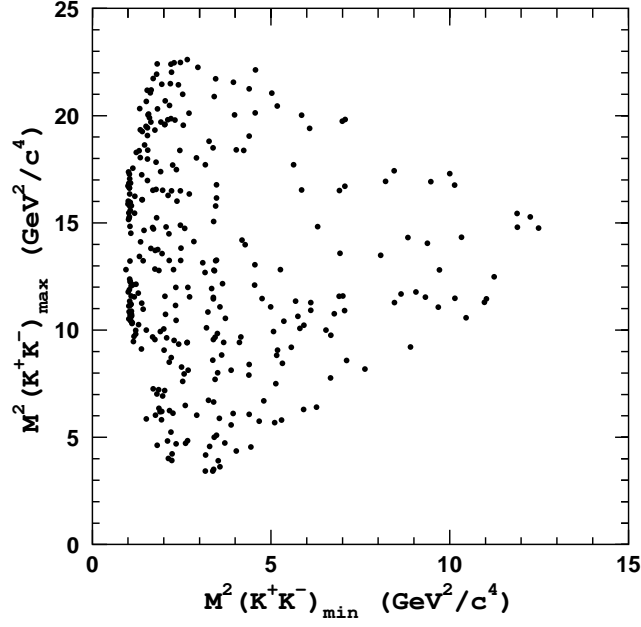


FIG. 4: The Dalitz plot for  $B^+ \rightarrow K^+K^+K^-$  candidates from the  $B$  signal region.

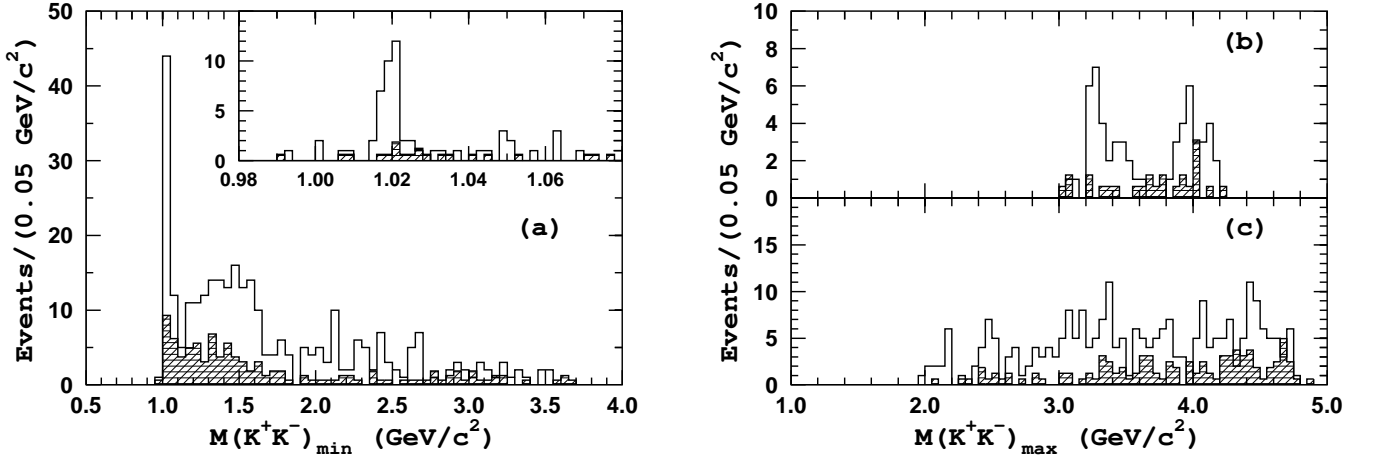


FIG. 5: The  $K^+K^-$  invariant mass spectra for selected  $B^+ \rightarrow K^+K^+K^-$  candidates in the  $B$  signal region (open histograms) and for background events in the  $\Delta E$  sidebands (hatched histograms). (a) The  $K^+K^-$  combination with the smaller invariant mass. The inset shows the  $\phi(1020)$  region in  $2 \text{ MeV}/c^2$  bins; (b) the  $M(K^+K^-)_{\text{max}}$  spectrum with  $M(K^+K^-)_{\text{min}} < 1.1 \text{ GeV}/c^2$  and (c) the  $M(K^+K^-)_{\text{max}}$  spectrum with  $M(K^+K^-)_{\text{min}} > 1.1 \text{ GeV}/c^2$ .

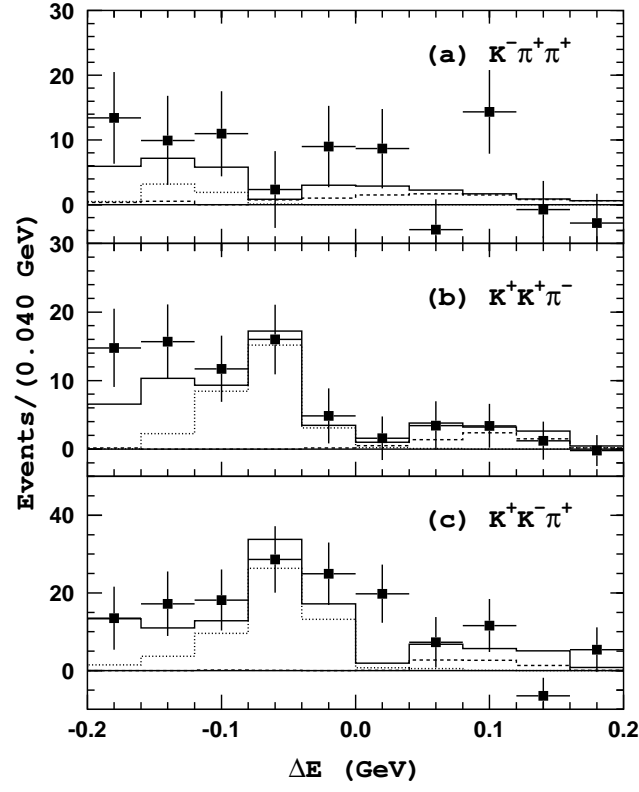


FIG. 6: Results of the fit to the  $M_{bc}$  distributions in  $\Delta E$  bins. The data (points with errors) are compared with the MC expectation (open histogram). The feed-down from  $K^+ K^+ K^-$  and  $K^+ \pi^+ \pi^-$  final states is shown by the dotted and dashed histograms, respectively.